Journal of Imaging Science and Technology® 61(4): 040407-1–040407-11, 2017.

N-LMMSE Demosaicing for Spectral Filter Arrays

Prakhar Amba▲
LPNC-UMR CNRS 5105, Université de Grenoble-Alpes, Grenoble, France
E-mail: prakhar.amba@univ-grenoble-alpes.fr

Jean Baptiste Thomas▲
The Norwegian Colour and Visual Computing Laboratory, NTNU, Gjøvik, Norway
Le2i, FRE CNRS 2005, Université de Bourgogne Franche-Comté, Dijon, France

David Alleysson▲
LPNC-UMR CNRS 5105, Université de Grenoble-Alpes, Grenoble, France

Abstract. *Spectral filter array (SFA) technology requires development on demosaicing. The authors extend the linear minimum mean square error with neighborhood method to the spectral dimension. They demonstrate that the method is fast and general on Raw SFA images that span the visible and near infra-red part of the electromagnetic range. The method is quantitatively evaluated in simulation first, then the authors evaluate it on real data by the use of non-reference image quality metrics applied on each band. Resulting images show a much better reconstruction of text and high frequencies at the expense of a zipping effect, compared to the benchmark binary-tree method.* © *2017 Society for Imaging Science and Technology.*
[DOI: 10.2352/J.ImagingSci.Technol.2017.61.4.040407]

INTRODUCTION

Spectral filter array technology (SFA)[1] provides, similarly to color filter arrays (CFA), a spatio-spectral, sparse description of an image of the scene. Spectral reconstruction addresses the recovery of the spectral information from multispectral data, e.g., Ref. 2, and is not the focus of this article. We focus on the reconstruction of the spatial information for each sensor spectral sensitivity, which is referred to as demosaicing.

SFA, such as most spectral imaging techniques, may be applied to different problems: high quality color imaging,[3] spectral reconstruction imaging[2] and generic computer vision.[4] Sensor design and data processing may be different depending on the application. According to our knowledge, the first work on filter array imaging dedicated to spectral imaging has been conducted by Ramanath et al.[5,6] Since then, several works have been conducted to develop this concept. Physical realization of SFA sensors are yet few. Although a limited number of companies started to commercialize the technology,[7–9] we identify only two prototypes embedded in actual cameras in the academic: One comes from the Le2i at Université de Bourgogne, Franche-Comté,[10] the other comes from Ukotomi & Tanaka Laboratory at the Tokyo Institute of Technology.[11] Interest of these realizations is that each of them comes with a database freely available online for research, SFA database spanning the visible and near infra-red (NIR)[12] and TokyoTech Multispectral Image dataset (http://www.ok.sc.e.titech.ac.jp/res/MSI/MSIdata.html).

Demosaicing was extensively studied for CFA, and particularly specialized on the Bayer layout.[13] See e.g., Refs. 14–18. However, scientific communications related to this problem are still published regularly.[19] Spectral sensitivities[20] and spatial layout[21–23] influence the demosaicing greatly. Other factors, such as optical aberrations,[24] also contribute.

SFA demosaicing has attracted interests, and in the last 2 years, we have seen a profusion of scientific communications dedicated to this specific problem. Some methods are extended from CFA based on the Bayer pattern, so they benefit from an oversampled band and are very compliant with Monno et al. sensor realization. Frequency-based approaches, such as spectral correlation,[25] high-frequency based,[26] discrete wavelet transform,[27] adaptive bilateral and Gaussian kernel upsampling,[28] guided filter,[29,30] spatial gradient and inter-channel correlation[31] demosaicings have been extended to SFA.

More general formulations have also been developed. Extension of the difference between channels have been considered.[32,33] Bilinear interpolation have also been implemented and upgraded into the binary-tree approach from Miao et al.,[34–36] as well as the vector median interpolation.[37]

Linear general formulations have shown great results, such as the spectral linear minimum mean square error (LMMSE),[38,39] RGB-NIR LMMSE,[40] linear reconstruction by training,[41–43] linear intensity-based demosaicing[44] and inter-channel correlation-based demosaicing[45] have been studied. And low-pass filtering in Fourier domain[46,47] was investigated.

Variational approaches have been extended to a vectorial formulation[48] with great success. Some investiga-

▲ IS&T Members.

Received Feb. 24, 2017; accepted for publication June 20, 2017; published online July 24, 2017. Associate Editor: Jang Jin Yoo.
1062-3701/2017/61(4)/040407/11/$25.00

tions that assume no correlations between bands have been developed,[49,50] within which some are based on super-resolution.[51,52] Compressive sensing to compensate for the increasing sparsity have also been used successfully.[53–55] Specific to technology, such as Fourier SFA[56,57] and hybrid multi-camera approaches[58] and specific to application demosaicing[59] have also been developed.

Solving different issues, such as noise or blur[60] was implemented jointly with the demosaicing. Color visualization of SFA images has been studied also to compensate demosaicing errors[61] or to compensate for spectral multiplexing between visible and NIR.[62]

Within this list of works, the first are a lot dependent on the SFA pattern, which impairs their generality. Among the others, most require heavy processing or iteration, which breaks the interesting potential of SFA for real-time robotic applications. One very interesting result recently published is the introduction of neighborhood in the LMMSE (N-LMMSE) formulation by Amba et al.[23] LMMSE has been developed for CFA[63–66] with great success. It has been proven to be a very good general solution in the evaluations[23,39] on both CFA and SFA. This formulation provides a potentially very good candidate for real-time applications since, after training, it could be embedded into the camera hardware and perform real time without losing the generality required by the different layouts present in the market.

Also, most of the works above have been evaluated on simulation. The challenge with real data is that there is no available ground truth to compare reconstruction with. Although in the case of color images, and potentially on spectral images in the visible, dedicated to accurate colorimetric rendering, we could consider psycho-visual ratings and rankings, when NIR data are present, it is more difficult to evaluate the result and color images makes no complete sense.

One way to evaluate demosaicing would be to provide a usability study on the available real data, assuming that the best result is provided by the best demosaicing method. Another possibility would be to assess the quality of the data in a general case. We propose to use **no-reference image quality metrics** to evaluate the demosaiced image quality, and to couple the analysis with a usual simulation on hyperspectral radiance reference data set. No-reference image quality metrics have already been used in this context for color images by Gasparini et al.,[67] but according to our knowledge, not on spectral data. As a first step toward this methodology, we use gray-level, general quality metrics applied by band in this work.

In next section, we develop the N-LMMSE demosaicing to spectral images. We then develop our experiment and evaluation procedure, which is based on real SFA images that span the visible and the NIR. Results demonstrate that the N-LMMSE method permits to reconstruct better fine details and in particular text and high frequency, however, it exhibits more zipping effect. Another observation is that energy balance, such as defined in Ref. 68 plays a role in the learning/reconstruction process of the LMMSE, which impairs in particular the NIR channel due to illumination shift between learning and training. This suggests that a white balance must be performed before demosaicing. No-reference metrics seems not well adapted for the NIR information and show different behavior depending on the image content and demosaicing. Further works are required to evaluate the quality of this evaluation process.

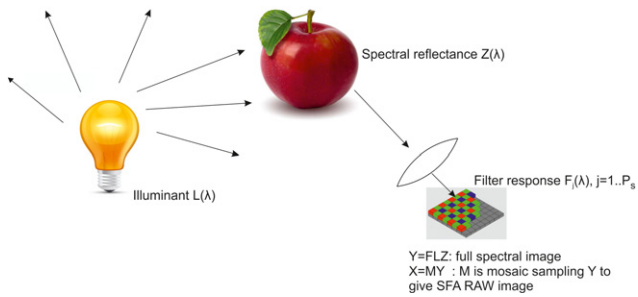

Figure 1. Image formation model from reflectance objects.

LINEAR MODEL FOR DEMOSAICING

Model of Linear SFA Image Formation

A reflectance model of image formation (Figure 1) considers a light source that has a spectral power distribution $L(\lambda)$, which illuminates a scene that has a spectral reflectance $Z(\lambda)$. The reflected spectra then passes through a camera lens, is acted upon by the spectral response $F_j(\lambda), j = 1..P_s$ of each spectral filter, where P_s are number of different spectral filters overlaid on the sensor. The signal is integrated and for a pixel covered by filter $F_j(\lambda)$, gives $\rho_j = \int F_j(\lambda)L(\lambda)Z(\lambda)\,\mathrm{d}\lambda$, $j = 1..P_s$. If each spectral filter covered the entire surface of the sensor (e.g., sequential acquisition with filter wheel) we would get a full resolution filtered image Y. However, in the case of SFA, Y is sampled by the filter mosaic $\boldsymbol{M}$ before hitting the silicon sensor to form the SFA raw image X. The goal of demosaicing algorithm is to estimate Y from X. Demosaicing algorithms exploit spatial and spectral correlations to guess the missing colors. Algorithms in the spatial domain adapted to Bayer-like layout estimate the *Green* channel first and then interpolate the other channels, by estimating the edges in horizontal or vertical direction. Alternatively in the frequency domain, luminance and spectral (alternatively chrominance in CFA) information are localized separately and it is a question of designing demosaicing filters to separate them.[66]

However, for SFAs we need to consider a generic spectral model as the spatial and spectral correlations for SFAs can be different from those for visible RGB camera. For RGB cameras filters are generally wideband and overlapping, spatial correlation is present in most of the bands. The SFAs may have narrow band spectral response and there maybe no overlap present; therefore, the spatial/spectral correlation is different. Also between visible and NIR filters, the spatial correlation is quite different due to difference in reflectance properties of objects for NIR. Therefore, we need a different class of algorithms to solve this problem. Demosaicing can be considered as an inverse problem and we can choose

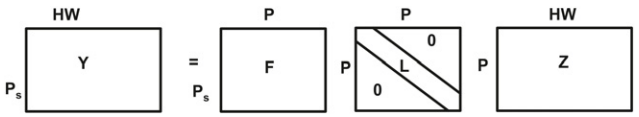

Figure 2. Illustration of image formation model on Reflectance images. For sake of comprehension we express 3D images Y and Z by unfolding them along HW. A projection by SFA applied to Y will give us SFA image X of size 1 x HW.

a solution on the criteria of minimizing the mean square error between the Y and an estimate $\hat{Y}$ derived from X. As the SFA basis pattern is repeated across the sensor surface, a block-shift invariant solution can be considered, which simplifies calculation. We consider a linear solution to this problem for simplicity. In most previous implementations, the size of Y was P_S times X; therefore, the solution was not very stable. Hence, we propose to add redundancy by using neighboring pixels in X, which leads to the N-LMMSE formulation.

N-LMMSE Formulation

To enable expression of image matrices and the illuminant, spectral filter response, and so forth, in a linear algebraic matrix multiplication terms we need to first unfold them into column vectors. We choose to do so in a block-shift invariant manner as we need the same demosaicing operation on each basis pattern of filter arrangement. A discrete physical measurement leads to a discrete representation of image reflectance Z, and scene illumination L over the spatial resolution of the sensor and its spectral sensitivity F by bands. This measurement Y is then subsampled by the mosaic to simulate the SFA image X.

Now X which is the SFA image is of size $H \times W$ where H and W are the number of rows and columns in the sensor. Similarly, Y which is a full-resolution spectral image of size HWP_s where P_s is the number of spectral filters present in the mosaic. If P_s spectral filters form the mosaic basis pattern of size $h \times w$, we can have at most $P_s \leq hw$. Now this basis pattern is repeated across the surface of the sensor to form the SFA.

Z is reflectance data typically defined for several wavelength bands P, i.e., Z has a size of HWP. F is the SPD for the P_S filters defined over a range of wavelength, i.e., F is of size P_s x P. F is typically specified by the camera manufacturers or can be measured using a monochromator and spectrophotometer. L is the SPD of the light source defined for P wavelength bands. We diagonalize this matrix, i.e., make it of size $P \times P$ to enable matrix product (Figure 2).

The relation between full resolution Y and X is defined by multiplication by a projection matrix $\boldsymbol{M}$. Now we consider the block-shift invariant property of the mosaic and unfold accordingly (Figure 3).

Since the mosaic is composed of basis pattern of size hw we can unfold each basis pattern into a column vector. So Z can be unfolded into a matrix $\boldsymbol{z}$ of size $Phw \times HW/hw$. Similarly for X which is unfolded to matrix $\boldsymbol{x}$ of size $hw \times HW/hw$. So y is unfolded color image in P_S channels of size $P_shw \times HW/hw$. L is also replicated across hw to a matrix $\boldsymbol{l}$ of size $Phw \times Phw$. F is replicated to a matrix $\boldsymbol{f}$ of size $P_shw \times Phw$. Finally $\boldsymbol{M}$ is the projection matrix of size $hw \times P_shw$.

Then we write:

$$y = flz \text{ and } x = My, \text{ so } x = Mflz.$$

The goal of the training is to estimate an operator D that when multiplied with x will give us an estimate of full resolution image $\hat{y}$:

$$\hat{y} = Dx \text{ such that } E_{i=1..k}\{(\hat{y} - y)^2\} \text{ is minimum}$$
$$\text{so } D = E_{i=1..k}\{(yx^t)(xx^t)^{-1}\}$$

D can be calculated from a database of reflectance images by learning of correlation between x and y pairs.

To enforce stability of solution we incorporate redundancy by considering neighborhood around the basis pattern in x and y, defined as x_1 and y_1 (Figure 4). Let z_1 be the matrix $\boldsymbol{z}$ considering a neighborhood of $n_h \times n_w$ pixels around each pixel in the basis pattern, i.e., we consider n_h pixels along height and n_w pixels along width direction. So z_1 will be of size $Phwn_hn_w \times HW/hw$. Similarly x_1 is of size $hwn_hn_w \times HW/hw$. By choosing a big neighborhood size we can ensure hwn_hn_w, i.e., element in x_1 is greater than P_shw i.e., element in y. We also need to expand f_1, l_1 and M_1 in similar fashion to incorporate neighborhood (Figure 5). It is also possible to design a matrix $\boldsymbol{S}_1$ which selects the central pattern in z_1. Then,

$$x_1 = M_1 f_1 l_1 z_1, \; z = \boldsymbol{S}_1 z_1 \text{ and } \hat{y} = Dx_1,$$
$$\text{with } D = E_{i=1..k}\{(yx_1^t)(x_1x_1^t)^{-1}\}$$
$$D = (flS_1Rl_1^tf_1^tM_1^t)(M_1f_1l_1Rl_1^tf_1^tM_1^t)^{-1},$$
$$\text{where } R = E_{i=1...k}\{(z_1z_1^t)\}.$$

Above equation implies that for a given database of reflectance images we need to learn the cross-correlation matrix $\boldsymbol{R}$ only once. We can then construct M_1 and S_1 for any given SFA arrangement, construct f_1 for filter SPDs and l_1 for any reference light to find the corresponding $\boldsymbol{D}$ matrix for demosaicing to recover the full resolution $\hat{Y}$ image.

EXPERIMENTS

Quantitative Analysis in Simulation

We simulate acquisition on the SCIEN (https://scien.stanford.edu/index.php/hyperspectral-image-data/) radiance image database,[69] following the model described above. We simulate acquisition by a real sensor(Figure 6) that spans visible and NIR,[10,70] where spatial layout follows Miao binary tree.[36,71,72] The benchmark demosaicing, Miao binary tree,[34] is applied on the raw data for reconstruction. Algorithms using guided filter and adaptive kernel[11] are tuned to SFAs having quincunx sampling of green so it would be non-efficient and unfair to compare with our instance of SFA. Also we considered the compressive sensing (Kronecker and Group-Sparse)[53] approach. The authors

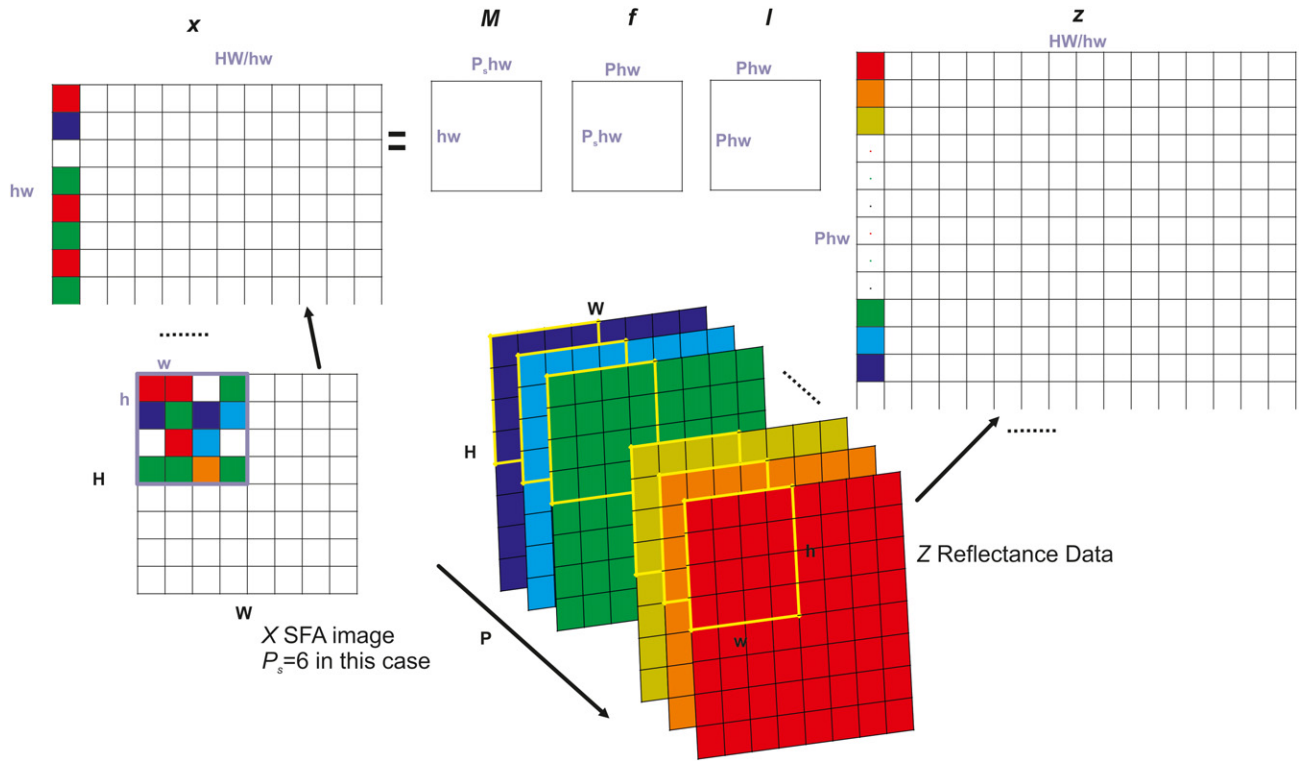

Figure 3. Linear matrix model of the SFA image formation without neighborhood. Reflectance images are not colored. Here they are artificially done to help the understanding of matrix unfolding.

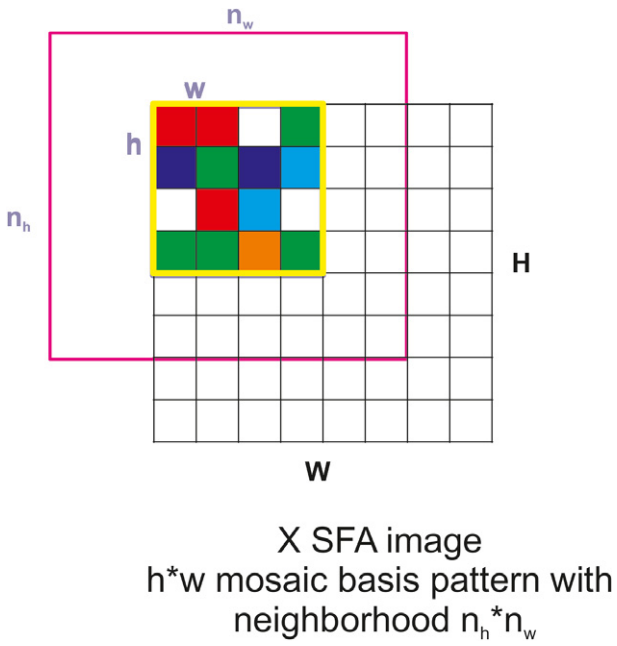

Figure 4. Illustration of neighborhood around basis pattern for SFA image X. We consider n_h pixels along height and n_w around width.

themselves state that this approach is more suited for random sampling of filters and not for uniform ones so it is not really fair to compare their method with our algorithm. Indeed, in physical implementations we usually do not have a totally random arrangement (entire sensor size) of SFAs. In testing on SCIEN images we found the performance of such methods (sPSNR) was worse than Miao binary tree for our SFA instantiation. Also this algorithm was 1400 times slower than N-LMMSE. For computer vision applications for which SFAs are particularly well suited and calculations on embedded systems, real-time performance is paramount for which we find Sparse-based solutions are not suited. Therefore, we choose not to present results from their method.

The N-LMMSE is trained and applied in a leave-one-out (LOO) manner on each of the images, while trained on the three others sequentially. We used a neighborhood of size 10 as it gives the best trade off between performance and computational complexity.[23] sPSNR and sSSIM[73] are used to compare the reconstructed image to the full resolution image. Results of PSNR and SSIM for the benchmark are reported in Table I, while results for the N-LMMSE are reported in Table II. The D operator when applied to SFA images, might give us negative or greater than 1 output values. We do not apply any non-negative constraints as of now and simply clip output values between 0 and 1. We observe a large gain of quality according to both PSNR and SSIM using N-LMMSE. With Binary Tree we get an average sPSNR value of 46.41 dB while N-LMMSE gives us 53.74 dB, i.e., a gain of 7.33 dB. The output images are also sharper. Similar average sSSIM goes up from 0.9959 to 0.9995.

In anticipation on the evaluation of real data, we also apply no-reference image quality metrics on each channel, considering that each channel is compliant with gray-level

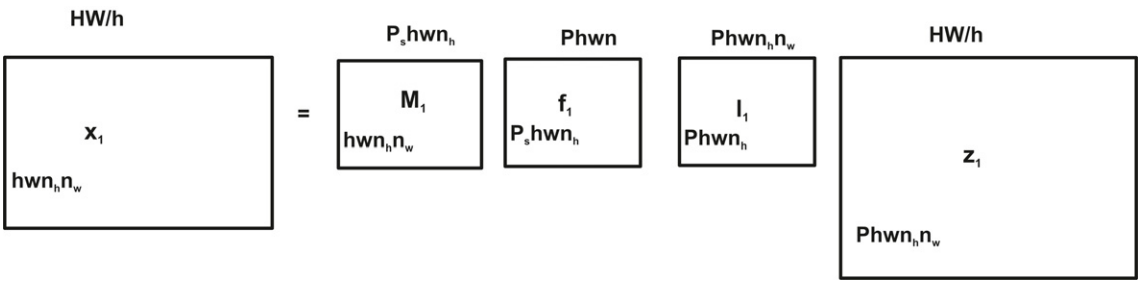

Figure 5. Illustration of linear matrix model of SFA image formation incorporating neighborhood.

Table I. Result of PSNR, SSIM, BLIIND-II and BRISQUE for reconstruction based on the benchmark binary-tree demosaicing applied to the simulated images from SCIEN database.

Scene name	BLIIND-II									BRISQUE								
	Average	S1	S2	S3	S4	S5	S6	S7	S8	Average	S1	S2	S3	S4	S5	S6	S7	S8
SanFrancisco	43.50	42.50	44.50	46.00	32.50	49.00	47.50	48.50	37.50	74.08	74.95	75.23	71.24	70.51	84.62	82.80	81.11	52.17
StanfordDish	38.38	39.50	42.00	40.50	29.00	40.00	36.50	46.50	33.00	67.04	67.29	67.24	65.55	64.07	73.14	72.63	74.34	52.05
StanfordMem.	62.00	73.00	66.50	61.50	49.50	64.00	64.50	84.50	32.50	83.55	88.45	87.04	84.54	81.39	89.07	87.78	94.58	55.57
StanfordTower	33.13	33.00	34.00	39.00	24.50	32.50	31.50	36.00	34.50	66.91	67.49	67.59	63.32	62.66	74.59	73.73	71.64	54.22
Average	44.25	47.00	46.75	46.75	33.88	46.38	45.00	53.88	34.38	72.89	74.54	74.28	71.16	69.66	80.36	79.23	80.42	53.50
Scene name	PSNR									SSIM								
	sPSNR	S1	S2	S3	S4	S5	S6	S7	S8	sSSIM	S1	S2	S3	S4	S5	S6	S7	S8
SanFrancisco	45.74	54.77	53.75	52.89	51.88	54.64	54.80	57.39	37.31	0.9958	0.9970	0.9965	0.9957	0.9950	0.9971	0.9971	0.9981	0.9290
StanfordDish	44.30	53.75	53.19	52.55	51.97	55.83	55.99	57.88	35.69	0.9954	0.9961	0.9959	0.9951	0.9945	0.9976	0.9976	0.9982	0.9229
StanfordMem.	52.80	58.84	57.36	56.90	55.97	58.65	58.91	61.93	45.09	0.9985	0.9991	0.9989	0.9988	0.9985	0.9990	0.9990	0.9994	0.9881
StanfordTower	42.79	51.87	50.92	49.77	48.71	51.82	52.01	54.28	34.37	0.9938	0.9945	0.9940	0.9925	0.9911	0.9950	0.9951	0.9964	0.8932
Average	46.41	54.81	53.80	53.03	52.13	55.24	55.43	57.87	38.11	0.9959	0.9967	0.9963	0.9955	0.9948	0.9972	0.9972	0.9980	0.9333

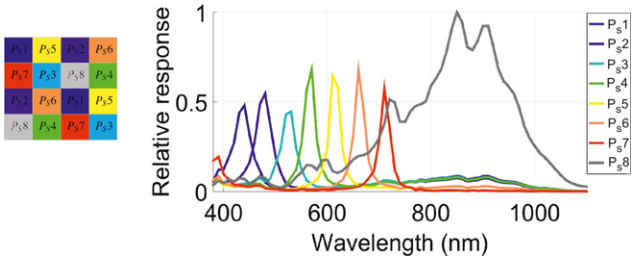

Figure 6. Spectral Filter Array (SFA) mosaic arrangement of filters & their spectral response for our camera.

natural image statistics. The no-reference metrics that we use on each band are supposedly representative of perceived visual quality. This is the most compact mean to perform the cumbersome task of evaluating perceived image quality on each channel. We selected arbitrarily (*ad hoc* choice after discussions with image quality experts) two metrics that appear to provide reasonably good estimate of quality in the general cases. The metrics are BRISQUE[74,75] and BLIINDS-II.[76,77] We used the implementations available at LIVE (http://live.ece.utexas.edu/research/Quality/index.htm). The only no-reference metric dedicated to demosaicing[67] focuses on color images, and thus, unfortunately, was not meeting our purpose of spectral image evaluation.

Results are reported on tables I and II. Both metrics show better quality with smaller values. For both BLIIND-II and BRISQUE, N-LMMSE provides better results with BRISQUE following better the PSNR and SSIM trend.

If we look at the correlation coefficient for the binary-tree algorithm we see that both BRISQUE and BLIINDS-II metrics are highly correlated with PSNR and SSIM for all the spectral channels other than the NIR. This is counter intuitive as in general we expect a negative correlation, higher PSNR means lower BRISQUE for example. The NIR channel not following the same trends indicates that these metrics are not suitable for the same. For the N-LMMSE method the correlation coefficient we see negative or weak correlation for most of the channels which is more as per expectation.

Analysis on Real Images

Real raw images from the same sensor are provided by the SFA (http://chic.u-bourgogne.fr/) database.[12] We applied on the raw data the binary-tree benchmark demosaicing method and the N-LMMSE method trained, this time, on the four images of the SCIEN database. Reconstruction example on one image is respectively provided on Figures 7 and 8. We observe visually that we gain spatial resolution, images are sharper with less false colors, and text is better reconstructed by the N-LMMSE method as compared with

Table II. Result of PSNR, SSIM, BLIIND-II and BRISQUE for reconstruction based on the N-LMMSE demosaicing applied to the simulated images from SCIEN database. We used a LOO method.

Scene name	BLIIND-II									BRISQUE								
	Average	S1	S2	S3	S4	S5	S6	S7	S8	Average	S1	S2	S3	S4	S5	S6	S7	S8
SanFrancisco	40.56	41.00	41.00	43.00	40.50	43.00	43.00	42.50	30.50	60.70	61.69	60.91	58.17	57.49	69.85	69.92	71.31	36.28
StanfordDish	35.00	39.50	37.50	35.00	32.00	35.50	32.50	40.00	28.00	51.74	54.23	52.26	50.10	47.92	57.78	58.17	61.99	31.46
StanfordMem.	51.50	58.50	52.50	50.00	30.50	61.00	59.50	72.00	28.00	64.84	72.77	68.88	65.72	62.26	70.06	70.20	79.91	28.94
StanfordTower	33.75	37.50	35.50	34.00	34.50	31.50	30.50	35.00	31.50	53.23	53.67	52.55	50.60	49.67	57.62	57.72	60.68	43.35
Average	40.20	44.13	41.63	40.50	34.38	42.75	41.38	47.38	29.50	57.63	60.59	58.65	56.15	54.34	63.83	64.00	68.47	35.01
Scene name	PSNR									SSIM								
	Average	S1	S2	S3	S4	S5	S6	S7	S8	Average	S1	S2	S3	S4	S5	S6	S7	S8
SanFrancisco	55.30	68.43	68.11	67.67	66.01	67.38	66.35	69.96	46.50	0.9996	0.9999	0.9999	0.9999	0.9998	0.9998	0.9998	0.9999	0.9915
StanfordDish	53.08	65.95	64.99	64.95	64.22	66.27	65.27	67.72	44.27	0.9995	0.9998	0.9998	0.9998	0.9997	0.9998	0.9997	0.9998	0.9891
StanfordMem.	54.63	64.71	61.92	62.05	60.40	63.31	64.21	67.56	46.20	0.9995	0.9998	0.9997	0.9996	0.9995	0.9997	0.9997	0.9999	0.9925
StanfordTower	51.96	65.05	64.46	64.22	62.16	64.23	63.13	66.34	43.17	0.9994	0.9997	0.9997	0.9997	0.9996	0.9997	0.9996	0.9998	0.9871
Average	53.74	66.04	64.87	64.72	63.20	65.30	64.74	67.89	45.04	0.9995	0.9998	0.9998	0.9997	0.9997	0.9998	0.9997	0.9998	0.9901

Figure 7. Binary-tree results on the 8 spectral channels.

the binary tree; however, there are some zipper artifacts in visible channels and NIR channel has lots of artifacts. There we observe one of the limitation of the methods that needs to learn compared to the interpolation methods in the sense that the changes of conditions and content between training and application could strongly impact the results. For the purpose of training here we have only four images available. The training would be more general if we could have a bigger dataset of differing conditions available. Also there is a difference in illumination of the test images (SCIEN Radiance data) which the model learns and the illumination in real images shot under a D65 simulator. Here, our result suggests that energy balance or spectral white balance[78] should be applied prior to demosaicing in the case of N-LMMSE method.

Worse results of N-LMMSE to the reconstruction of the NIR for the real images are due to statistics of real images which are artificial materials shot indoor not being similar to those used for learning from the SCIEN database. If we look at the spectral response curves of the filters it is clear that the NIR filter higher sensitivity compared to other filters. If we simulate on SCIEN it translates into on average 10 times more compared to the "deep red" filter and similarly for other filters. This is what the *D* operator learns. Whereas in the real images captured by the camera the NIR channel is only 5.8 times more sensitive so the demosaiced result is not good. Other channels maintain similar ratios in the simulated and real data so demosaicing works well for them.

Also there is possibly another reason for the degrading NIR performance. In Appendix A of Ref. 10, the authors have

Figure 8. N-LMMSE results on the 8 spectral channels.

Figure 9. Visualization of SFA images demosaiced by the binary tree and rendered in sRGB space.

provided the spectral response of all the pixels on the sensor. We see a rather large variance in the NIR channel compared to other filters. What our model learns is an average response of these pixels; therefore, there is a difference between what the model predicts and actual RAW images from the camera. For the zipper artifacts we have two issues, one is the spatial resolution allowed by the SFA pattern which could limit the performance of our demosaicing operator. We also see there is variability in spectral response for even the color filters, which could also create artifacts even in visible channels. Generally for RGB cameras available commercially we do not have such intra-channel variability and therefore we do not have such artifacts with N-LMMSE. Again these are hypothetical explanations.

Other demosaiced images show similar tendency and are available at this link (http://chic.u-bourgogne.fr/).

We apply the two no-reference metrics BLIIND-II and BRISQUE on each of the reconstructed channels, which are considered as gray-level images. Results are shown in Table III for the binary tree and in Table IV for the N-LMMSE. With the N-LMMSE approach the values for NIR channel are either zero or negative, which it is not clear on how to interpret. However, we know that these metrics may not be suitable for the NIR channel. Similarly for the BLIIND-II some of the other spectral channels report zero value which is again unclear as to the relation with other channels. In general the values for both the metrics are lower for N-LMMSE compared to binary tree which implies that it is better at reconstructing the spectral channels. This can be collaborated with visual inspection of image channels. However, at the moment the relation between reference and no-reference metrics is not so clear with respect to our

Table III. Result of reconstruction for the benchmark binary tree applied to the real SFA images.

Scene name	BLIIND-II									BRISQUE								
	Average	S1	S2	S3	S4	S5	S6	S7	S8	Average	S1	S2	S3	S4	S5	S6	S7	S8
Battery	36.44	39.00	43.00	35.50	37.00	34.50	30.50	29.00	43.00	57.54	59.50	60.29	59.63	56.06	56.22	55.46	61.14	52.06
Black Swimsuit	33.50	36.50	36.00	34.50	32.00	31.50	33.50	20.50	43.50	83.18	84.21	86.31	86.04	86.99	83.33	82.85	79.10	76.64
CD	31.63	33.00	39.50	40.50	34.00	30.00	25.00	13.50	37.50	53.10	55.71	52.87	54.25	51.47	55.12	54.76	55.67	44.93
Kerchief	44.13	44.50	49.50	48.00	50.00	48.00	45.50	31.00	36.50	59.65	45.00	61.96	82.39	76.24	55.49	47.47	64.06	44.56
Kiwi	29.88	26.50	29.50	28.00	30.50	32.50	38.00	15.00	39.00	52.85	62.96	57.56	53.67	51.58	49.90	50.36	60.23	36.53
Knife	33.31	36.00	38.00	40.00	34.00	30.50	26.50	13.50	48.00	45.86	51.43	47.69	46.18	50.95	50.40	38.93	40.29	41.05
Macbeth	32.44	34.00	33.50	34.00	29.50	28.00	32.50	25.00	43.00	65.65	64.84	63.00	63.05	63.29	66.75	68.59	71.92	63.79
Orange	21.00	18.00	18.50	20.50	22.00	27.00	22.00	13.50	26.50	64.00	65.67	67.81	66.51	65.90	64.74	66.33	65.36	49.73
Origan	33.31	31.00	33.00	35.00	32.00	30.00	35.00	31.50	39.00	52.95	54.97	56.21	49.32	55.99	52.16	52.99	56.18	45.78
Painting	25.25	30.00	26.00	26.00	30.50	28.50	24.50	11.00	25.50	46.95	52.76	47.64	50.26	48.71	40.80	48.55	51.72	35.13
Pastel	48.31	42.00	44.00	61.00	60.50	51.50	40.50	34.50	52.50	71.07	70.75	70.64	73.38	71.62	72.65	73.56	68.04	67.94
Pens	50.19	45.50	47.50	50.00	48.00	54.50	51.00	37.50	67.50	66.62	65.28	65.86	63.96	63.56	68.72	71.97	70.27	63.32
Raspberry	36.56	34.00	42.50	30.00	33.50	36.00	40.00	32.50	44.00	60.96	63.29	65.18	61.14	62.82	58.70	57.51	57.30	61.78
Ruler	31.94	29.50	44.00	41.50	35.50	32.50	23.00	13.00	36.50	53.24	52.77	50.07	52.51	52.69	55.08	58.70	61.21	42.85
SD	24.00	22.50	24.50	26.50	27.50	25.00	25.00	15.00	26.00	52.00	52.53	50.04	53.80	52.50	50.88	53.86	57.46	44.92
Train Front	29.69	27.50	28.00	30.50	31.50	30.50	32.00	21.50	36.00	64.58	66.37	62.80	63.65	63.94	66.66	70.23	70.52	52.50
Train Side	24.44	28.50	27.00	27.50	30.50	25.50	21.00	11.00	24.50	70.23	72.06	71.79	69.10	66.36	72.37	73.84	74.01	62.29
Water	37.81	43.50	50.00	43.00	36.00	33.00	26.50	24.50	46.00	57.22	61.28	57.25	58.41	55.92	55.83	59.95	61.15	47.99
Average	33.55	33.42	36.33	36.22	35.25	33.83	31.78	21.83	39.69	59.87	61.19	60.83	61.51	60.92	59.77	60.33	62.53	51.88
Median	32.88	33.50	37.00	34.75	32.75	31.00	31.25	21.00	39.00	58.60	62.12	61.12	60.38	59.44	56.02	58.11	61.18	48.86

Table IV. Result of reconstruction for the N-LMMSE applied to the real SFA images.

Scene name	BLIIND-II									BRISQUE								
	Average	S1	S2	S3	S4	S5	S6	S7	S8	Average	S1	S2	S3	S4	S5	S6	S7	S8
Battery	16.19	16.00	22.50	21.00	19.50	16.50	15.50	18.50	0.00	12.37	19.42	20.52	16.95	14.89	14.48	10.37	13.86	-11.50
Black Swimsuit	20.56	12.50	29.50	17.50	22.50	37.50	27.00	17.50	0.50	43.26	47.77	47.39	47.09	44.70	50.83	50.58	49.19	8.50
CD	17.38	18.50	28.00	25.50	20.50	19.00	15.50	12.00	0.00	14.06	16.72	18.49	18.00	18.52	15.01	13.64	20.08	-7.97
Kerchief	25.00	22.50	32.00	27.00	27.50	31.50	30.00	29.50	0.00	45.85	44.04	65.06	64.98	73.07	52.84	44.73	43.89	-21.79
Kiwi	14.88	3.00	13.00	8.50	12.50	25.00	28.00	29.00	0.00	17.63	23.47	19.29	18.08	16.78	21.46	23.55	31.67	-13.28
Knife	16.25	15.50	23.50	20.00	17.50	26.50	14.00	13.00	0.00	15.56	17.24	21.29	19.05	16.26	18.35	18.80	18.92	-5.44
Macbeth	8.00	2.00	11.50	9.00	1.50	13.50	9.50	17.00	0.00	40.72	44.98	46.91	47.00	47.15	44.07	43.81	47.01	4.84
Orange	6.75	0.00	0.00	0.00	0.00	14.50	17.00	22.50	0.00	139.23	138.36	156.53	157.11	157.34	157.14	151.30	121.47	74.59
Origan	11.56	9.00	16.50	14.50	10.50	9.00	13.50	19.50	0.00	8.77	11.32	9.37	7.92	6.12	11.11	12.16	20.81	-8.66
Painting	11.88	5.00	12.50	6.50	14.50	18.00	18.00	20.50	0.00	21.43	27.17	32.33	31.29	30.56	26.62	23.03	20.59	-20.13
Pastel	18.06	7.00	0.00	27.50	31.00	30.50	22.00	26.50	0.00	32.97	39.40	43.47	39.19	36.56	33.58	31.91	34.11	5.51
Pens	19.00	6.50	24.50	18.00	18.00	29.50	27.00	28.50	0.00	24.25	28.57	24.46	22.16	19.55	27.29	28.84	43.87	-0.73
Raspberry	13.00	8.00	14.50	14.50	13.50	23.00	17.00	13.50	0.00	14.69	17.63	17.57	17.28	17.61	18.00	18.12	22.56	-11.29
Ruler	15.81	13.50	24.00	21.00	14.50	17.00	15.50	21.00	0.00	14.30	18.15	22.54	23.93	25.07	19.57	16.79	19.08	-30.73
SD	8.63	0.00	8.00	1.00	0.00	20.50	20.00	19.50	0.00	23.09	21.72	29.28	30.45	36.06	30.17	29.09	21.04	-13.09
Train Front	6.31	0.00	13.00	0.00	0.00	9.50	16.50	11.50	0.00	29.61	35.44	35.06	34.82	34.19	31.86	31.45	40.45	-6.39
Train Side	7.38	2.00	10.50	5.00	0.00	9.00	20.50	12.00	0.00	18.18	30.04	26.49	23.06	18.16	12.82	18.41	32.48	-15.99
Water	25.06	26.50	36.00	31.50	26.50	30.50	22.50	27.00	0.00	20.44	22.05	23.15	24.06	24.86	26.76	25.69	27.51	-10.61
Average	14.54	9.31	17.75	14.89	13.89	21.14	19.39	19.92	0.03	29.80	33.53	36.62	35.69	35.41	34.00	32.90	34.92	-4.68
Median	15.34	7.50	15.50	16.00	14.50	19.75	17.50	19.50	0.00	20.93	25.32	25.48	24.00	24.97	26.69	24.62	29.59	-9.63

Figure 10. Visualization of SFA images demosaiced by N-LMMSE and rendered in sRGB space.

evaluation on SCIEN images and more work is required to clearly identify their relation.

Visualization of Color Images

In order to visualize images and provide digestive qualitative visual results, we visualize a colorimetric version of the images. We use the Wiener filtering approach to define the linear transform T_{FtoXYZ}, such as $T_{FtoXYZ} = (XYZ)F(FF^t)^{-1}$, which projects the image data from F to the XYZ space, where XYZ are defined by the *CIE* 1931 for the standard observer. This transform is applied to the image data such as $Y_{XYZ} = T_{FtoXYZ}Y$. Then, we use the *CIE XYZ* to *sRGB* transform to obtain the display image $Y_{sRGB} = XYZ$ to $sRGB(Y_{XYZ})$.

Color versions of the database are shown in Figure 9 for binary tree and in Figure 10 for the N-LMMSE. Note also that the color version of these images are different from Ref. 12 because a different color transform was used. On these images, we first observe, that the N-LMMSE exhibits some spectral noise, graininess, which is more prominent than in the case of the binary tree, which provides smoother images. We observe again that high frequencies are better reconstructed by the N-LMMSE. This is particularly clear on any of the texts and on the ruler graduations. Color artifacts are also quite well avoided by the N-LMMSE, but a closer look shows zipping effect while binary tree is preserved thanks to its directional interpolation aspect. Although the zipping effect is problematic, we have however gained spatial resolution. Still it is important to remember that this is a sensor with eight different filters with different relative sensitivities and in addition intra-pixel variability in spectral response.

Color visualization limits the influence of the NIR component, which is not very well reconstructed by the N-LMMSE, but still provide a general overview of the performance.

CONCLUSION

In conclusion, we have extended the N-LMMSE framework from the RGB color to the spectral domain. We found that N-LMMSE provides good results in terms of PSNR & SSIM for such SFA layout which we demonstrate on image simulated from SCIEN hyperspectral database and also validated on real RAW images. In particular, it provides good reconstruction of text and high-frequency components, but shows limited performance in the object edge, whereas the binary tree provides a blurred but unzipped image. Looking at sPSNR and sSSIM numbers of simulated SCIEN images, we find a significant gain compared to binary-tree approach. Also N-LMMSE being a linear method is computationally simple compared to compressive sensing/sparse solutions and therefore is suitable for real-time applications. We used no-reference metrics on each band which are supposedly representative of perceived visual quality of individual bands. It is yet difficult to understand the results of the no-reference metrics, which seem to depend greatly on the image content, in particular BLIIND-II, which may not be suitable for this evaluation. This work shows also the dependency of reconstruction algorithms to the illumination as compared to interpolation algorithms, which have no such priors. This may be further evaluated in future work.

ACKNOWLEDGMENT

This work is financed by the FUI Extrem OWL no. F1411026U and ANR LACIS ANR-14-CE26-0034 to P. Amba and D. Alleysson. Also by EU-project, H2020-662222, EXIST http://cordis.europa.eu/project/rcn/198017_en.html to J.-B. Thomas.

REFERENCES

[1] P.-J. Lapray, X. Wang, J.-B. Thomas, and P. Gouton, "Multispectral filter arrays: Recent advances and practical implementation," Sensors **14**, 21626 (2014) ISSN: 1424-8220. doi: 10.3390/s141121626. URL http://www.mdpi.com/1424-8220/14/11/21626.

[2] X. Wang, J.-B. Thomas, J. Y. Hardeberg, and P. Gouton, "Multispectral imaging: narrow or wide band filters?," J. Int. Colour Assoc. **12**, 44–51 (2014).

[3] X. Wang, P. J. Green, J.-B. Thomas, J. Y. Hardeberg, and P. Gouton, *Evaluation of the Colorimetric Performance of Single-Sensor Image Acquisition Systems Employing Colour and Multispectral Filter Array* (Springer International Publishing, Cham, 2015), pp. 181–191, ISBN: 978-3-319-15979-9. doi: 10.1007/978-3-319-15979-9_18. URL http://dx.doi.org/10.1007/978-3-319-15979-9_18.

[4] Y. Benezeth, D. Sidibé, and J.-B. Thomas, "Background subtraction with multispectral video sequences," *IEEE ICRA Workshops* (IEEE, Piscataway, NJ, 2014), p. 6, URL http://hal-univ-bourgogne.archives-ouvertes.fr/hal-00986168.

[5] R. Ramanath, W. E. Snyder, G. L. Bilbro, and W. A. Sander, (2001) "Robust multispectral imaging sensors for autonomous robots," Technical Report, North Carolina State University (2011), Retrieved 16 June 2014. 10.1117/12.543418. URL http://dx.doi.org/10.1117/12.543418.

[6] R. Ramanath, W. E. Snyder, and H. Qi, "Mosaic multispectral focal plane array cameras," Proc. SPIE **5406**, 701–712 (2004).

[7] IMEC. hyperspectral-imaging. URL http://www2.imec.be.

[8] SILIOS-TECHNOLOGIES. Micro-optics supplier. URL http://www.silios.com/.

[9] PIXELTEQ. "Micro-patterned optical filters. URL https://pixelteq.com/.

[10] J.-B. Thomas, P.-J. Lapray, P. Gouton, and C. Clerc, "Spectral characterization of a prototype SFA camera for joint visible and NIR acquisition," Sensors **16**, 993 (2016) ISSN: 1424-8220. doi: 10.3390/s16070993. URL http://www.mdpi.com/1424-8220/16/7/993.

[11] Y. Monno, S. Kikuchi, M. Tanaka, and M. Okutomi, "A practical one-shot multispectral imaging system using a single image sensor," IEEE Trans Image Process. **24**, 3048–3059 (2015) ISSN: 1057-7149. doi: 10.1109/TIP.2015.2436342.

[12] P.-J. Lapray, J.-B. Thomas, and P. Gouton, "A database of spectral filter array images that combine visible and nir," *6th Computational Color Imaging Workshop, CCIW'17* (2017).

[13] B. E. Bayer, "Color imaging array" US Patent 3,971,065 (1976) URL http://www.google.com/patents/US3971065.

[14] R. Ramanath, W. E. Snyder, G. L. Bilbro, and W. A. Sander III, "Demosaicking methods for bayer color arrays," J. Electron. Imaging **11**, 306–315 (2002).

[15] B. K. Gunturk, J. Glotzbach, Y. Altunbasak, R. W. Schafer, and R. M. Mersereau, "Demosaicking: color filter array interpolation," Signal Process. Mag. **22**, 44–54 (2005).

[16] X. Li, B. Gunturk, and L. Zhang, "Image demosaicing: a systematic survey," Proc. SPIE **6822**, 68221J (2008).

[17] O. Losson, L. Macaire, and Y. Yang, "Comparison of color demosaicing methods," *Advances in Imaging and Electron Physics*, edited by P. Hawkes (Elsevier, 2010), Vol. 162, chapter 5, pp. 173–265.

[18] D. Menon and G. Calvagno, "Color image demosaicking: An overview," Image Commun. **26**, 518–533 (2011) ISSN: 0923-5965. doi: 10.1016/j.image.2011.04.003. URL http://dx.doi.org/10.1016/j.image.2011.04.003.

[19] M. R. Nazari, "*Denoising and Demosaicking of Color Images*," Ph.D. thesis (Electrical Engineering and Computer Science, Université d'Ottawa, Ontario, Canada, (2017). PhD in Engineering.

[20] M. Parmar and S. J. Reeves, "Selection of optimal spectral sensitivity functions for color filter arrays," IEEE Trans. Image Process. **19**, 3190–3203 (2010).

[21] Y. M. Lu and M. Vetterli, "Optimal color filter array design: Quantitative conditions and an efficient search procedure," Proc. SPIE **7250**, 725009 (2009).

[22] D. Alleysson, B. C. De Lavarene, and J. Herault, "Digital image sensor, image capture and reconstruction method and system for implementing same," US Patent 8,564,699 (2013). URL http://www.google.ch/patents/US8564699.

[23] P. Amba, J. Dias, and D. Alleysson, "Random color filter arrays are better than regular ones," J. Imaging Sci. Technol. **60**, 50406-1 (2016).

[24] X. Wang, M. Pedersen, and J.-B. Thomas, "The influence of chromatic aberration on demosaicking," *5th European Workshop on Visual Information Processing (EUVIP)* (IEEE, Piscataway, NJ, 2014), pp. 1–6, doi: 10.1109/EUVIP.2014.7018410.

[25] S. P. Jaiswal, L. Fang, V. Jakhetiya, J. Pang, K. Mueller, and O. C. Au, "Adaptive multispectral demosaicking based on frequency-domain analysis of spectral correlation," IEEE Trans. Image Process. **26**, 953–968 (2017) ISSN: 1057-7149. doi: 10.1109/TIP.2016.2634120.

[26] S. P. Jaiswal, L. Fang, V. Jakhetiya, M. Kuse, and O. C. Au, "Optimized high-frequency based interpolation for multispectral demosaicking," *2016 IEEE Int'l. Conf. Image Processing (ICIP)* (IEEE, Piscataway, NJ, 2016), pp. 2851–2855.

[27] X. Wang, J.-B. Thomas, J. Y. Hardeberg, and P. Gouton, "Discrete wavelet transform based multispectral filter array demosaicking," *Proc. Colour and Visual Computing Symposium (CVCS), 2013* (2013), pp. 1–6, doi: 10.1109/CVCS.2013.6626274.

[28] Y. Monno, M. Tanaka, and M. Okutomi, "Multispectral demosaicking using adaptive kernel upsampling," *18th IEEE Int'l. Conf. Image Processing (ICIP)* (IEEE, Piscataway, NJ, 2011), pp. 3157–3160.

[29] Y. Monno, M. Tanakaa, and M. Okutomia, "Multispectral demosaicking using guided filter," Proc. SPIE **8299**, 82990O (2012).

[30] Y. Monno, D. Kiku, S. Kikuchi, M. Tanaka, and M. Okutomi, "Multispectral demosaicking with novel guide image generation and residual interpolation," *2014 IEEE Int'l. Conf. on Image Processing (ICIP)* (IEEE, Piscataway, NJ, 2014), pp. 645–649, doi: 10.1109/ICIP.2014.7025129.

[31] S. Ogawa, K. Shinoda, M. Hasegawa, S. Kato, M. Ishikawa, H. Komagata, and N. Kobayashi, *Demosaicking Method for Multispectral Images Based on Spatial Gradient and Inter-channel Correlation* (Springer International Publishing, Cham, 2016), pp. 157–166, ISBN: 978-3-319-33618-3. doi: 10.1007/978-3-319-33618-3_17. URL http://dx.doi.org/10.1007/978-3-319-33618-3_17.

[32] J. Brauers and T. Aach, "A color filter array based multispectral camera," *12th Workshop Farbbildverarbeitung*, edited by German Color Group (Ilmenau, 2006).

[33] S. Mihoubi, O. Losson, B. Mathon, and L. Macaire, "Multispectral demosaicing using intensity in edge-sensing and iterative difference-based methods," *IEEE SITIS 2016, Proc. 12th Int'l. IEEE Conf. on Signal Image Technology & Internet Based Systems* (IEEE, Piscataway, NJ, 2016), pp. 805–810, doi: 10.1109/SITIS.2016.132. URL https://hal.archives-ouvertes.fr/hal-01409705 (December).

[34] L. Miao, H. Qi, R. Ramanath, and W. E. Snyder, "Binary tree-based generic demosaicking algorithm for multispectral filter arrays," IEEE Trans. Image Process. **15**, 3550–3558 (2006) ISSN: 1057-7149. doi: 10.1109/TIP.2006.877476.

[35] L. Miao, H. Qi, and R. Ramanath, "A generic binary tree-based progressive demosaicking method for multispectral filter array," *Int'l. Conf. Image Processing (ICIP)* (IEEE, Piscataway, NJ, 2006), pp. 3221–3224, doi: 10.1109/ICIP.2006.312909.

[36] L. Miao, H. Qi, and R. Ramanath, "Generic msfa mosaicking and demosaicking for multispectral cameras," Proc. SPIE **6069**, 606909 (2006) doi: 10.1117/12.642366. URL: http://dx.doi.org/10.1117/12.642366.

[37] X. Wang, J.-B. Thomas, J. Y. Hardeberg, and P. Gouton, "Median filtering in multispectral filter array demosaicking," Proc. SPIE **8660**, 86600E (2013) doi: 10.1117/12.2005256. URL http://dx.doi.org/10.1117/12.2005256 (February).

[38] C. Wang, X. Wang, and J. Y. Hardeberg, "A linear interpolation algorithm for spectral filter array demosaicking," *Image and Signal Processing*, edited by A. Elmoataz, O. Lezoray, F. Nouboud, and D. Mammass, Lecture Notes in Computer Science (Springer International Publishing, 2014), Vol. 8509, pp. 151–160, ISBN: 978-3-319-07997-4. doi: 10.1007/978-3-319-07998-1_18. URL http://dx.doi.org/10.1007/978-3-319-07998-1_18.

[39] X. Wang, "*Filter Array Based Spectral Imaging: Demosaicing and Design Considerations*." Ph.D. thesis, (LE2I-UBFC, The colorlab-NTNU, 2016).

[40] Y. Lu, C. Fredembach, M. Vetterli, and S. Süsstrunk, "Designing color filter arrays for the joint capture of visible and near-infrared images," *16th IEEE Int'l. Conf. Image Processing (ICIP)* (IEEE, Piscataway, NJ, 2009), pp. 3797–3800, doi: 10.1109/ICIP.2009.5414324.

[41] H. K. Aggarwal, A. Majumdar, and R. Ward, "A reconstruction algorithm for multi-spectral image demosaicing," *IASTED Signal and Image Processing* (2013).

[42] H. K. Aggarwal and A. Majumdar, "Multi-spectral demosaicing technique for single-sensor imaging," *Fourth National Conf. on Computer Vision, Pattern Recognition, Image Processing and Graphics (NCVPRIPG), 2013* (2013), pp. 1–4, doi: 10.1109/NCVPRIPG.2013.6776236.

[43] H. K. Aggarwal and A. Majumdar, "Single-sensor multi-spectral image demosaicing algorithm using learned interpolation weights," *Proc. Int'l. Geoscience and Remote Sensing Symposium (IGARSS), 2014* (2014).

[44] S. Mihoubi, O. Losson, B. Mathon, and L. Macaire, "Multispectral demosaicing using intensity-based spectral correlation," *2015 Int'l. Conf. Image Processing Theory, Tools and Applications (IPTA)* (2015), pp. 461–466, doi: 10.1109/IPTA.2015.7367188.

[45] J. Mizutani, S. Ogawa, K. Shinoda, M. Hasegawa, and S. Kato, "Multispectral demosaicking algorithm based on inter-channel correlation," *2014 IEEE Visual Communications and Image Processing Conf.* (IEEE, Piscataway, NJ, 2014), pp. 474–477, doi: 10.1109/VCIP.2014.7051609.

[46] F. Yasuma, T. Mitsunaga, D. Iso, and S. K. Nayar, "Generalized assorted pixel camera: Post-capture control of resolution, dynamic range and spectrum," Technical Report, Department of Computer Science, Columbia University CUCS-061-08, (Nov. 2008) http://www1.cs.columbia.edu/CAVE/databases/multispectral/.

[47] F. Yasuma, T. Mitsunaga, D. Iso, and S. K. Nayar, "Generalized assorted pixel camera: Postcapture control of resolution, dynamic range, and spectrum," IEEE Trans. Image Process. **19**, 2241–2253 (2010) ISSN: 1057-7149. doi: 10.1109/TIP.2010.2046811.

[48] K. Shinoda, T. Hamasaki, M. Kawase, M. Hasegawa, and S. Kato, "Demosaicking for multispectral images based on vectorial total variation," Opt. Rev. **23**, 559–570 (2016) ISSN: 1349-9432. doi: 10.1007/s10043-016-0221-y. URL http://dx.doi.org/10.1007/s10043-016-0221-y.

[49] D. Kiku, Y. Monno, M. Tanaka, and M. Okutomi, "Simultaneous capturing of rgb and additional band images using hybrid color filter array," Proc. SPIE **9023**, 90230V (2014) doi: 10.1117/12.2039396. URL http://dx.doi.org/10.1117/12.2039396.

[50] A. V. Kanaev, M. Rawhouser, M. R. Kutteruf, M. K. Yetzbacher, M. J. De Prenger, K. M. Novak, C. A. Miller, and C. W. Miller, "Demosaicking for full motion video 9-band swir sensor," Proc. SPIE **9104**, 910407 (2014) doi: 10.1117/12.2051223. URL http://dx.doi.org/10.1117/12.2051223.

[51] A. V. Kanaev, "Demosaicking system and method for color array based multi-spectral sensors," US Patent 9,336,570 (2016) URL https://www.google.com/patents/US9336570.

[52] A. Kanaev, M. Kutteruf, M. Yetzbacher, M. Deprenger, K. Novak, and C. Miller, "Increasing resolution of multi-spectral mosaic-array cameras," *Imaging and Applied Optics* (Optical Society of America, 2015), 2015, p. IT2A.5, doi: 10.1117/12.2051223. URL http://www.osapublishing.org/abstract.cfm?URI=ISA-2015-IT2A.5.

[53] H. K. Aggarwal and A. Majumdar, "Compressive sensing multi-spectral demosaicing from single sensor architecture," *Proc. 2nd IEEE China Summit and Int'l. Conf. Signal and Information Processing (ChinaSIP), 2014* (IEEE, Piscataway, NJ, 2014).

[54] H. K. Aggarwal and A. Majumdar, "Multi-spectral demosaicing: A joint-sparse elastic-net formulation," *2015 Eighth Int'l. Conf. on Advances in Pattern Recognition (ICAPR)* (2015), pp. 1–5, doi 10.1109/ICAPR.2015.7050649.

[55] Y. H. Mejia-Melgarejo, O. P. Villarreal-Dulcey, and H. Arguello-Fuentes, "Adjustable spatial resolution of compressive spectral images sensed by multispectral filter array-based sensors," Revista Facultad de IngenierÃa Universidad de Antioquia 89–98 (2016) ISSN: 0120-6230. URL http://www.scielo.org.co/scielo.php?script=sci_arttext&pid=S0120-62302016000100012&nrm=iso.

[56] J. Jia and K. Hirakawa, "Single-shot fourier transform multispectroscopy," *2015 IEEE Int'l. Conf. Image Processing (ICIP)* (IEEE, Piscataway, NJ, 2015), pp. 4205–4209, doi: 10.1109/ICIP.2015.7351598.

[57] J. Jia, C. Ni, A. Sarangan, and K. Hirakawa, "Guided filter demosaicking for fourier spectral filter array," *IS&T Electronic Imaging: Visual Information Processing and Communication VII* (IS&T, Springfield, VA, 2016), pp. 1–5, ISSN: 2470-1173. doi: 10.2352/ISSN.2470-1173.2016.2.VIPC-228. URL http://www.ingentaconnect.com/content/ist/ei/2016/00002016/00000002/art00004.

[58] Y. Murakami, M. Yamaguchi, and N. Ohyama, "Hybrid-resolution multispectral imaging using color filter array," Opt. Express **20**, 7173–7183 (2012) doi: 10.1364/OE.20.007173. URL http://www.opticsexpress.org/abstract.cfm?URI=oe-20-7-7173.

[59] K. Shinoda, S. Ogawa, Y. Yanagi, M. Hasegawa, S. Kato, M. Ishikawa, H. Komagata, and N. Kobayashi, "Multispectral filter array and demosaicking for pathological images," *2015 Asia-Pacific Signal and Information Processing Association Annual Summit and Conf. (APSIPA)* (2015), pp. 697–703, doi: 10.1109/APSIPA.2015.7415362.

[60] J. Y. Kwon and M. G. Kang, "Multispectral demosaicking considering out-of-focus problem for red-green-blue-near-infrared image sensors," J. Electron. Imaging **25**, 023010 (2016) doi: 10.1117/1.JEI.25.2.023010. URL http://dx.doi.org/10.1117/1.JEI.25.2.023010.

[61] Y. Monno, M. Tanaka, and M. Okutomi, "N-to-srgb mapping for single-sensor multispectral imaging," *IEEE Int'l. Conf. Computer Vision (ICCV) Workshops* (IEEE, Piscataway, NJ, 2015).

[62] Z. Sadeghipoor, J.-B. Thomas, and S. Süsstrunk, "Demultiplexing visible and near-infrared information in single-sensor multispectral imaging," *Proc. IS&T CIC24: Twenty-fourth Color and Imaging Conf.* (IS&T, Springfield, VA, 2016), pp. 76–81.

[63] D. Taubman, "Generalized wiener reconstruction of images from colour sensor data using a scale invariant prior," *Image Processing, 2000. Proc. 2000 Int'. Conf.* (IEEE, Piscataway, NJ, 2000), Vol. 3, pp. 801–804.

[64] H. J. Trussell, "A mmse estimate for demosaicking," *Image Processing, 2001. Proc. 2001 Int'l. Conf. Image Processing (ICIP)* (IEEE, Piscataway, NJ, 2001), Vol. 3, pp. 358–361.

[65] H. J. Trussell and R. E. Hartwig, "Mathematics for demosaicking," IEEE Trans. Image Process. **11**, 485–492 (2002).

[66] D. Alleysson, S. Susstrunk, and J. Hérault, "Linear demosaicing inspired by the human visual system," IEEE Trans. Image Process. **14**, 439–449 (2005).

[67] F. Gasparini, F. Marini, R. Schettini, and M. Guarnera, "A no-reference metric for demosaicing artifacts that fits psycho-visual experiments," EURASIP J. Adv. Signal Processing **2012**, 123 (2012) ISSN: 1687-6180. doi: 10.1186/1687-6180-2012-123. URL http://dx.doi.org/10.1186/1687-6180-2012-123.

[68] P.-J. Lapray, J.-B. Thomas, P. Gouton, and Y. Ruichek, "Energy balance in spectral filter array camera design," J. Eur. Optical Society-Rapid Publications **13**, 1 (2017) ISSN: 1990-2573. doi: 10.1186/s41476-016-0031-7. URL http://dx.doi.org/10.1186/s41476-016-0031-7.

[69] T. Skauli and J. Farrell, "A collection of hyperspectral images for imaging systems research," Proc. SPIE **8660**, 86600C (2013) doi: 10.1117/12.2007097. URL http://dx.doi.org/10.1117/12.2007097.

[70] P.-J. Lapray, J.-B. Thomas, and P. Gouton, "A multispectral acquisition system using msfas," *Proc. IS&T CIC22: Twenty-second Color and Imaging Conf.* (IS&T, Springfield, VA, 2014), Vol. 2014, pp. 97–102, URL http://www.ingentaconnect.com/content/ist/cic/2014/00002014/00002014/art00016.

[71] L. Miao, H. Qi, and W. E. Snyder, "A generic method for generating multispectral filter arrays," *Int'l. Conf. Image Processing (ICIP)* (IEEE, Piscataway, NJ, 2004), Vol. 5, pp. 3343–3346, doi 10.1109/ICIP.2004.1421830.

[72] L. Miao and H. Qi, "The design and evaluation of a generic method for generating mosaicked multispectral filter arrays," IEEE Trans. Image Process. **15**, 2780–2791 (2006) ISSN: 1057-7149. doi 10.1109/TIP.2006.877315.

[73] Z. Wang, A. C. Bovik, H. R. Sheikh, and E. P. Simoncelli, "Image quality assessment: from error visibility to structural similarity," IEEE Trans. Image Process. **13**, 600–612 (2004).

[74] A. MLA Mittal, A. K. Moorthy, and A. C. Bovik, "Referenceless image spatial quality evaluation engine," *45th Asilomar Conference on Signals, Systems and Computers* (2011).

[75] A. Mittal, A. K. Moorthy, and A. C. Bovik, "No-reference image quality assessment in the spatial domain," IEEE Trans. Image Process. **21**, 4695–4708 (2012) ISSN: 1057-7149. doi: 10.1109/TIP.2006.877315.

[76] M. A. Saad, A. C. Bovik, and C. Charrier, "Dct statistics model-based blind image quality assessment," *2011 18th IEEE Int'l. Conf. Image Processing (ICIP)* (IEEE, Piscataway, NJ, 2011), pp. 3093–3096, doi: 10.1109/ICIP.2011.6116319.

[77] M. A. Saad, A. C. Bovik, and C. Charrier, "Blind image quality assessment: A natural scene statistics approach in the dct domain," IEEE Trans. Image Process. **21**, 3339–3352 (2012) ISSN: 1057-7149. doi: 10.1109/TIP.2012.2191563.

[78] J. B. Thomas, "Illuminant estimation from uncalibrated multispectral images," *2015 Colour and Visual Computing Symposium (CVCS)* (2015), pp. 1–6, doi 10.1109/CVCS.2015.7274900.